Interaction of a dielectric waveguide mode with a resonant scatterer: Scattering properties, propelling force, and torque

A. V. Maslov
Department of Radiophysics, University of Nizhny Novgorod, Nizhny Novgorod 603022, Russia

(Received 23 August 2021; accepted 22 March 2022; published 7 April 2022)

A system of a resonant scatterer described as a two-level atom coupled to a circular dielectric waveguide is studied. The system is characterized by the scattering properties of a guided mode (guided transmission and reflection, bulk radiation) and optomechanical properties (propelling force and torque on the scatterer). The results are based on a self-consistent solution of the scattering problem using the Green's functions and cover the cases of scatterers inside and outside waveguides. It is shown that while a scatterer with a fixed dipole orientation gives rise to scattering spectra described by Lorentzian line shapes, an isotropic scatterer can produce non-Lorentzian line shapes. The parameters defining the line shape are analyzed. The complicated line shapes are likely to arise in the coherent characterization of an emerging class of photonic devices based on photon emitters coupled to well-confined modes of dielectric waveguides. It is obtained that the propelling force and axial torque on the scatterer at resonance can be directly expressed in terms of the spontaneous emission coupling factor (β) of the system. The balances of the linear and angular momentum in the system are discussed. Numerical results are presented for strongly confined guided modes which allow efficient mode scattering and conversion of the linear and angular mode momentum to the force and torque, respectively.

DOI: 10.1103/PhysRevA.105.043503

I. INTRODUCTION

Small resonant elements (metal and high-index dielectric particles, molecules, atoms, impurities, quantum dots) located near or inside a waveguide can greatly scatter an incident guided mode. The pronounced scattering is somewhat surprising given the deeply subwavelength size of the scatterer and takes place for strongly confined modes with the transverse size comparable to the wavelength. What is more important, however, is that the scattered waves can stay inside the waveguide, rather than leave it. This creates realistic opportunities for optomechanical manipulation of resonant elements and for realizing various optical processing functions.

Initially, the interest in such coupled structures was due to the possibility of launching single photons from small emitters directly to waveguides. Currently, such structures are expected to find much broader applications as building blocks of complex systems as required, for example, for quantum networks. This stimulated the investigation of structures made of various emitters and waveguides: single organic molecules in glass capillary [1], single molecules near an on-chip waveguide [2], color centers in diamond coupled to nanowaveguides [3,4], atoms near optical nanofibers [5], quantum dots in photonic nanowires [6], and quantum dots coupled to photonic crystal waveguides [7]. The scattering of a guided mode on a single atom is attractive for obtaining strong nonlinearities [8,9], which can lead to the creation of a single-photon transistor [10]. Particles inside waveguides can also be used for optical modulation [11,12].

One of the current challenges in this developing technology is a reliable characterization of the interaction between the emitter and the waveguide. In the single mode regime, the interaction is typically described using two basic parameters: the fraction of the power emitted into the guided mode (β factor) and the enhancement of the emission rate into the guided mode compared to that in the bulk material (Purcell factor). There are several experimental methods for such characterization. One can measure the β factor by comparing the decay rate of an emitter coupled to the waveguide mode to that without the coupling [7]. One can also extract the coupling efficiency using extinction spectroscopy for a molecule inside a waveguide [1] or inside the cavity formed by an interrupted waveguide [13]. There are experimental measurements of the alignment-dependent decay rate of an atomic dipole near an optical nanofiber which partially agree with theoretical predictions [14].

The strong optical interaction between resonant particles and guided modes offers the possibility not only to manipulate light but also to move scatterers themselves by the optical forces. Often, the experiments show rather weak propulsion efficiency due to the lack of any resonant enhancement, for example, the propulsion of atoms inside hollow-core fibers [15] or particles by guided modes [16–18]. The resonant enhancement was obtained for large particles with whispering gallery mode (WGM) resonances, the excitation of which produces giant propelling forces with magnitudes comparable to the incident guided momentum [19,20]. If the propulsion by guided light is not desired, the longitudinal trapping can be achieved by using counterpropagating waves. Besides the force, guided light can create a torque on an atom near an optical nanofiber [21]. The interaction of guided modes with atoms can be used as a probe of the guided light angular

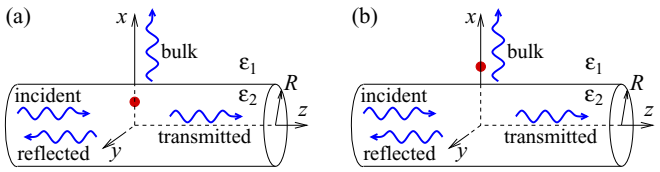

FIG. 1. Scattering of a guided mode by a particle (a) inside or (b) outside a dielectric wire with radius R and permittivity ε_2 surrounded by a medium with ε_1.

momentum and helicity [22]. Various metamaterial structures can also be used for creating optical torque [23–25] or optical pulling forces [26].

In this paper, we study the system of a resonant scatterer coupled to a circular dielectric waveguide. Both the optical and optomechanical properties are investigated with the purpose of creating a thorough understanding of the manifestation of the optical interaction in this system. We analyze the transformation of the incident power into newly created guided and bulk waves as well as the transformation of the incident linear and angular momentum into the force and torque, respectively. The scattering problem is solved self-consistently using the Green's function formalism. The key parameters of an emitter-waveguide system are the β factor and the Purcell factor. The β factor becomes rather large if the guided mode is well confined. This usually requires the use of high index waveguides, the modes of which have large axial electric fields. These factors define not only the emission properties but also the coherent scattering of a guided mode, which can be used for extracting these factors. However, the extraction procedure is simple only for the case of a specific orientation of the dipole transition. It is shown that for an isotropic scatterer complicated line shapes are likely to arise due to coherent superposition of the waves excited by the orthogonal components of the scatterer polarization. The force acting on the scatterer is analyzed using several approaches, which give identical results. A simple formula expressing the force in terms of the β factor is obtained. A similar analysis is performed for the axial torque and its value is also expressed in terms of the β factor.

This paper is organized as follows. Section II defines the problem and presents theoretical approaches to calculate the fields, force, and torque. Section III initially analyzes the efficiency of dipole emission into guided modes and overall modification of the emission rate, then it analyzes the scattering properties, force, and torque. Section IV gives conclusions.

II. SCATTERING PROBLEM AND ITS SOLUTION

A. Problem formulation and solution procedure

We consider the interaction of a mode guided by a dielectric waveguide (wire) with radius R and a resonant scatterer (particle) located at $x = x_0$ either inside ($x_0 < R$) or outside ($x_0 > R$) – see Fig. 1. The permittivity of the wire is ε_2 and that of the surrounding medium is ε_1. The scatterer is assumed to be much smaller than the wavelength and described by some polarizability $\chi_0(\omega)$. The scattering of the guided mode leads to the creation of various guided modes propagating in the $\pm z$ directions and bulk waves leaving the wire. We are interested in finding the scattering properties as well as the propelling force and axial torque on the scatterer. We will analyze both $x_0 < R$ and $x_0 > R$ in order to get a full picture of the interaction. Certainly, for $x_0 < R$ the force and torque on the scatterer will not result in its motion unless the dielectric is liquid. While the theoretical approach presented below is general, the interest lies primarily in a resonant scatterer and single mode guiding regime.

The solution is obtained in two steps. The first step is solving the problem of radiation emission by a point polarization source interacting with a waveguide. This allows relating the guided and bulk waves as well as the local field to the source polarization. The second step is adopting a specific model for the scatterer and finding its actual polarization using the calculated local field. The knowledge of the actual polarization immediately gives the amplitudes of the excited guided waves (and hence the transmission and reflection) as well as the bulk radiation. One can also use a slightly different approach. By solving the emission problem one can parametrize the results in terms of the β factor and the Purcell factor. This allows expressing the transmission, reflection, and bulk scattering in terms of these electromagnetic parameters and of the parameters of the scatterer. Both approaches are discussed.

We will use the Gaussian units. All true fields are assumed to vary sinusoidally at an angular frequency ω and are written in terms of complex amplitudes such as

$$\mathbf{E}(\mathbf{r}, t) = \mathbf{E}(\mathbf{r})e^{-i\omega t} + \mathbf{E}^*(\mathbf{r})e^{+i\omega t}. \tag{1}$$

This definition affects the formulas for the time-averaged energy, power, momentum, and force expressed in terms of the complex amplitudes of the field or polarization.

B. Properties of guided modes and their scattering

The incident wave is a guided mode of the wire. Quasicircularly polarized modes behave as $e^{in\varphi}$, where n is the azimuthal number and φ is the azimuthal angle. The lowest, or fundamental, modes have $n = \pm 1$ and the regime in which no other modes can exist is referred to as the single mode regime. The presence of a point scatterer at $x = x_0$ breaks the angular symmetry and, in general, leads to the excitation of guided waves with angular numbers which can differ from that of the incident. For example, the incidence of the $n = +1$ mode on a point scatterer leads to the excitation of the $n = -1$ mode. The intermode conversion can be avoided if the incident mode has quasilinear polarization, which is obtained by combining the $n = +1$ and -1 modes, and the scatterer polarization is coupled to one of the quasilinearly polarized modes only. For simplicity, we will refer to the modes as circular or linear without using the prefix *quasi*. The linear modes have the following angular dependence for the electric-field components:

$$x \text{ polarized}, \{E_\rho, E_\varphi, E_z\} \sim \{\cos\varphi, \sin\varphi, \cos\varphi\}; \tag{2a}$$

$$y \text{ polarized}, \{E_\rho, E_\varphi, E_z\} \sim \{\sin\varphi, \cos\varphi, \sin\varphi\}. \tag{2b}$$

At $\varphi = 0$, where the scatterer is located (see Fig. 1), the electric field of the y-polarized mode has only the φ component; the electric field of the x-polarized mode has only ρ and z components. If no intermode conversion takes place for the

linear modes, one can conveniently study the interaction of each of them with the scatterer separately. Specific conditions on the scatterer to avoid the intermode conversion are discussed in Secs. II C and II D.

Let us discuss the properties of guided modes which are relevant for characterizing the scattering as well as for finding the force and torque. A guided mode at some frequency ω can be characterized by its wave number $h_g > 0$ so that its complex fields behave as $e^{\pm i h_g z - i\omega t}$, where the $\pm$ signs describe the propagation in the $\pm z$ directions. The phase velocity is $v_{\rm ph} = \omega/h_g = c/n_{\rm ph}$ and the group velocity is $v_{\rm gr} = \partial\omega/\partial h_g = c/n_{\rm gr}$, where $n_{\rm ph}$ is the phase index and $n_{\rm gr}$ is the group index.

The propagation of a guided electromagnetic mode is associated with the storage of energy, linear momentum, and angular momentum as well as with the flow of the corresponding quantities. We can define the stored quantities per unit length (linear densities): energy $\mathcal{W}$, linear momentum $\mathcal{G}$, and angular momentum $\mathcal{J}$. We can also define the corresponding fluxes through a plane perpendicular to the waveguide axis: the energy flux (power) P, linear momentum flux M, and angular momentum flux J. We can express these quantities (averaged over time) in terms of the complex amplitudes [see also Eq. (1)].

The z and φ components of the Poynting vector are

$$S_z = \frac{c}{2\pi}\mathrm{Re}[E_\rho H_\varphi^* - E_\varphi H_\rho^*], \tag{3a}$$

$$S_\varphi = \frac{c}{2\pi}\mathrm{Re}[E_z H_\rho^* - E_\rho H_z^*]. \tag{3b}$$

Defining the cross-sectional integration as

$$\int d\sigma \; = \int_0^\infty \rho d\rho \int_0^{2\pi} d\varphi \tag{4}$$

and using (3) we express the energy $\mathcal{W}$, linear momentum $\mathcal{G}$, and angular momentum $\mathcal{J}$:

$$\mathcal{W} = \int d\sigma \; \frac{1}{4\pi}\left(\varepsilon|\mathbf{E}|^2 + |\mathbf{H}|^2\right), \tag{5a}$$

$$\mathcal{G} = \frac{1}{c^2}\int d\sigma \; \varepsilon S_z, \tag{5b}$$

$$\mathcal{J} = \frac{1}{c^2}\int d\sigma \; \rho\varepsilon S_\varphi, \tag{5c}$$

where ε is the radially dependent permittivity. We assume that $\varepsilon_{1,2}$ are dispersionless but the results can be directly generalized to account for dispersion. Note that the linear momentum in Eq. (5b) [and similarly the angular momentum in Eq. (5c)] is the so-called pseudomomentum (or Minkowski momentum) [27–29] (see also Sec. II F 1).

Using the Poynting vector (3a) for the power P and the stress tensor for the linear M and angular J momentum flux we obtain

$$P = \int d\sigma \; S_z, \tag{6a}$$

$$M = -\int d\sigma \; T_{zz}, \tag{6b}$$

$$J = -\int d\sigma \; \frac{\rho}{2\pi}\mathrm{Re}[\varepsilon E_\varphi E_z^* + H_\varphi H_z^*], \tag{6c}$$

where T_{zz} is the stress tensor component

$$T_{zz} = \frac{1}{4\pi}[2\varepsilon|E_z|^2 + 2|H_z|^2 - \varepsilon|\mathbf{E}|^2 - |\mathbf{H}|^2] \tag{7}$$

and the expression for J was simplified using the angular symmetry.

The fluxes P, M, and J are related to the corresponding stored quantities $\mathcal{W}$, $\mathcal{G}$, and $\mathcal{J}$ by

$$\frac{P}{\mathcal{W}} = \frac{M}{\mathcal{G}} = \frac{J}{\mathcal{J}} = v_{\rm gr} = \frac{c}{n_{\rm gr}}. \tag{8}$$

The energy $\mathcal{W}$ and linear momentum $\mathcal{G}$ (and their fluxes P and M) are related by

$$\frac{\mathcal{G}}{\mathcal{W}} = \frac{M}{P} = \frac{1}{v_{\rm ph}} = \frac{n_{\rm ph}}{c}. \tag{9}$$

The angular momentum for linearly polarized modes is zero. For a circularly polarized mode with azimuthal number n, the energy $\mathcal{W}$ and angular momentum $\mathcal{J}$ (and their fluxes P and J) are related by

$$\frac{\mathcal{J}}{\mathcal{W}} = \frac{J}{P} = \frac{n}{\omega}. \tag{10}$$

Relation (10) for the angular momentum in the Minkowski formulation can be considered as a classical analog of quantization of the circularly polarized angular momentum of a guided photon [22,30]. Relations (8)–(10) were verified numerically in the present paper. The linear and angular momentum fluxes can be used to find the force and torque on the scatterer as discussed in Sec. II F.

C. Dipole emission and local field

Let us find the fields produced by a pointlike source located at x_0 on the x axis (see Fig. 1):

$$\mathbf{P}(\mathbf{r}, \omega) = \mathbf{p}(\omega)\delta(\rho - x_0)\delta(\varphi)\delta(z)/\rho. \tag{11}$$

It is convenient to represent this pointlike polarization (or corresponding current) as a superposition of surface polarizations of cylindrical surfaces with $\rho = x_0$ using the following two expansions:

$$\delta(\varphi) = \frac{1}{2\pi}\sum_{n=-\infty}^{\infty} e^{in\varphi}, \quad \delta(z) = \frac{1}{2\pi}\int_{-\infty}^{+\infty} dh \; e^{ihz}. \tag{12}$$

Similar expansions are applied to all electromagnetic field components. For example, for $E_z(\rho, \varphi, z)$ we can write

$$E_z(\rho, \varphi, z) = \sum_{n=-\infty}^{\infty} E_z^n(\rho, z) e^{in\varphi}, \tag{13}$$

$$E_z^n(\rho, z) = \int_{-\infty}^{+\infty} dh \; \tilde{E}_z^n(\rho, h) e^{ihz}. \tag{14}$$

Each spatial component of $\mathbf{P}(\mathbf{r}, \omega)$ specified by h and n excites fields in the uniform regions defined by ε_1 and ε_2. These fields can be written using the cylindrical functions with some unknown coefficients. The coefficients can be calculated by matching the fields by the boundary conditions. The radiated

fields are then calculated by taking the inverse Fourier transform, Eq. (14), and adding all n components, Eq. (13). The integration path in Eq. (14) includes poles that correspond to the excitation of guided waves. The details of the integration can be found, for example, in Ref. [31].

The integration in the complex plane allows finding the electric field at any location, or the Green's function. In particular, one can calculate the field at the source location. The local field can be used to find the emitted power and the actual polarization $\mathbf{p}(\omega)$ in Eq. (11) from the scatterer polarizability. The local field induced by the scatterer can be written as a sum of two components:

$$\mathbf{E}^{\text{ind}} = \mathbf{E}^{\text{sf}} + \mathbf{E}^{\text{int}}, \tag{15}$$

where $\mathbf{E}^{\text{sf}}$ is the field that would be created by the scatterer in the uniform medium defined by the local permittivity and $\mathbf{E}^{\text{int}}$ is the additional field due to the interaction with the wire boundaries.

The self-induced field in Eq. (15) is

$$\mathbf{E}^{\text{sf}} = G^{(0)}\mathbf{p}, \tag{16}$$

where $G^{(0)}$ is the Green's function for the uniform medium with permittivity equal to that at the source location. We only need the imaginary part of $G^{(0)}$ to describe the intrinsic radiative damping:

$$\text{Im } G^{(0)} = g_v\sqrt{\varepsilon}, \quad g_v = \tfrac{2}{3}k^3, \tag{17}$$

where ε is the permittivity at the dipole location and $k = \omega/c$. The dipole in vacuum emits the power

$$P_v = 2\omega g_v |p|^2, \tag{18}$$

which will be used for normalizing powers later.

The ith vector component of the interaction field in Eq. (15) can be written using the tensor form of the Green's function $G_{ij}^{(1)}$ as

$$E_i^{\text{int}} = \sum_j G_{ij}^{(1)} p_j, \quad i, j = \rho, \varphi, z. \tag{19}$$

Here and in formulas later the subscript index i should not be confused with the imaginary unit i. Due to symmetry of the problem, only the diagonal components $G_{ii}^{(1)}$ are nonzeros. This means that for a dipole oriented along one of the basis directions (defined by the local basis vectors $\hat{\boldsymbol{\rho}}$, $\hat{\boldsymbol{\varphi}}$, $\hat{\mathbf{z}}$) the polarization will have the same components as the electric field of the incident guided mode. As a result, there will be no intermode conversion between the linearly polarized modes with angular dependencies given by Eq. (2).

Using the radiated fields one can find the power emitted into the bulk and guided modes by the polarization source (11). In particular, for the guided power one can use the reciprocity theorem to find the power carried by a specific mode propagating in the $\pm z$ direction:

$$P_g^{\pm} = -i\omega(\mathbf{p}^* \cdot \mathbf{E}_g^{\pm}), \tag{20}$$

where $\mathbf{E}_g^{\pm}$ is the field of the excited mode at the source location. This field can be evaluated directly by taking the corresponding residue. Note that expression (20) is always real.

The total emitted power is

$$P_{\text{tot}} = 2\omega \,\text{Im}(\mathbf{p}^* \cdot \mathbf{E}^{\text{ind}}). \tag{21}$$

Assuming that the dipole is oriented along one of the basis directions, P_{tot} can be written using (16)–(19) as

$$\frac{P_{\text{tot}}}{P_v} = \sqrt{\varepsilon} + \frac{\text{Im } G_{ii}^{(1)}}{g_v}. \tag{22}$$

The knowledge of the power emitted into the guided waves $P_g = P_g^+ + P_g^-$ and the total emitted power $P_{\text{tot}} = P_g + P_b$, which consists of the guided P_g and bulk P_b powers, allows finding the β factor

$$\beta = \frac{P_g}{P_{\text{tot}}} \tag{23}$$

and the Purcell factor

$$F_{\text{P}} = \frac{P_g}{\sqrt{\varepsilon}P_v} = \beta\frac{P_{\text{tot}}}{\sqrt{\varepsilon}P_v}, \tag{24}$$

where ε is the permittivity of the medium surrounding the dipole source (ε_1 for $x_0 > R$ or ε_2 for $x_0 < R$) and $\sqrt{\varepsilon}P_v$ is the power that would be emitted in a uniform dielectric with permittivity ε.

D. Two-level scatterer

1. General formulas for polarizability

In order to find the polarization amplitude $\mathbf{p}(\omega)$ in Eq. (11) we need to consider a specific model for the scatterer. Here we adopt the quantum-mechanical two-level model (atom) in which the scatterer is described by the following wave function:

$$|\Psi\rangle = A(t)|0\rangle + B(t)|1\rangle, \tag{25}$$

where $|0\rangle$ is the ground state, $|1\rangle$ is the excited state, and $A(t)$ and $B(t)$ are time-varying coefficients. Using (25) one can express the expectation value for the dipole moment:

$$\langle\Psi|\hat{\mathbf{d}}|\Psi\rangle = A^*B\mathbf{d} + \text{c.c.} = \mathbf{p}(t) + \text{c.c.}, \tag{26}$$

where $\mathbf{p}(t) = \mathbf{d}A^*(t)B(t)$ is the complex polarization and $\mathbf{d} = \langle 0|\hat{\mathbf{d}}|1\rangle$ is the transition dipole moment. The Schrödinger equation for $|\Psi\rangle$ is obtained using the interaction part of the Hamiltonian $\hat{\mathbf{d}}\mathbf{E}_s(t)$, where $\mathbf{E}_s(t)$ is the true field at the scatterer. Differentiating $\mathbf{p}(t)$ and using the Schrödinger equation we obtain

$$\frac{d\mathbf{p}}{dt} = -i\omega_0\mathbf{p} + i\frac{\mathbf{d}(\mathbf{d}^* \cdot \mathbf{E}_s)}{\hbar}(|A|^2 - |B|^2), \tag{27}$$

where ω_0 is the frequency difference between the states. In the linear regime, $|A| \approx 1$ and $|B| \ll |A|$, Eq. (27) reduces to

$$\frac{d\mathbf{p}}{dt} = -i\omega_0\mathbf{p} + i\frac{\mathbf{d}(\mathbf{d}^* \cdot \mathbf{E}_s)}{\hbar}. \tag{28}$$

For the electric field at the scatterer location

$$\mathbf{E}_s(t) = \mathbf{E}e^{-i\omega t} + \text{c.c.}, \tag{29}$$

we obtain in the rotating-wave approximation the following polarization:

$$\mathbf{p} = -\frac{\mathbf{d}(\mathbf{d}^* \cdot \mathbf{E})}{\hbar(\omega - \omega_0)}. \tag{30}$$

The complex amplitude in Eq. (30)

$$\mathbf{E} = \mathbf{E}^{\text{inc}} + \mathbf{E}^{\text{ind}} \tag{31}$$

includes the field of the incident guided mode $\mathbf{E}^{\text{inc}}$ and the field induced by the scatterer $\mathbf{E}^{\text{ind}}$. Let us now consider several specific cases which are of main interest in practice.

2. Scatterer oriented along a basis direction

Let us take a scatterer with the dipole moment along one of $\hat{\boldsymbol{\rho}}$, $\hat{\boldsymbol{\varphi}}$, or $\hat{\mathbf{z}}$. Substituting the electric fields (16) and (19) into the expression for the polarization (30) one obtains

$$p_i = -\frac{|\mathbf{d}|^2}{\hbar(\omega-\omega_0)}\left[E_i^{\text{inc}} + \left(G^{(0)} + G_{ii}^{(1)}\right)p_i\right], \tag{32}$$

where $i = \rho, \varphi, z$ and we used the condition $G_{ij}^{(1)} = 0$ if $i \neq j$. Using Eq. (32) we express p_i in terms of the incident field E_i^{inc} only:

$$p_i = \chi_i E_i^{\text{inc}}, \tag{33}$$

where the polarizability is

$$\chi_i(\omega) = -\frac{\gamma_v}{g_v(\omega-\omega_0-\delta_i+i\gamma_i)}. \tag{34}$$

The subscript i here denotes the orientation of the transition dipole moment. The frequency shift δ_i and radiative decay γ_i in (34) are given by

$$\frac{\delta_i}{\gamma_v} = -\frac{\text{Re}\, G_{ii}^{(1)}}{g_v}, \quad \frac{\gamma_i}{\gamma_v} = \frac{P_{\text{tot}}}{P_v} = \sqrt{\varepsilon} + \frac{\text{Im}\, G_{ii}^{(1)}}{g_v}, \tag{35}$$

where $\gamma_v = g_v|d|^2/\hbar$ is the decay rate for the polarization amplitude in vacuum. Note that we neglected the contribution of the self-field to the frequency shift. Equations (35) show that the normalized changes of the resonant frequency and linewidth depend only on the electromagnetic environment, that is, the Green's functions evaluated at the resonance, and not on the dipole moment.

3. Isotropic scatterer

An isotropic scatterer can be represented as an atom which has three possible transitions with the dipole moments oriented along the three basis directions. This means that, in general, the induced polarization is

$$\mathbf{p} = \hat{\boldsymbol{\rho}}\chi_\rho E_\rho^{\text{inc}} + \hat{\boldsymbol{\varphi}}\chi_\varphi E_\varphi^{\text{inc}} + \hat{\mathbf{z}}\chi_z E_z^{\text{inc}}, \tag{36}$$

where the responses χ_i are independent from each other and defined by Eqs. (34) and (35). The model of an isotropic scatterer is also applicable to Mie resonances in high-index microspheres [32].

4. Scatterer oriented along an arbitrary direction

Let us now take a scatterer with an arbitrary orientation of its dipole moment. To find the response, we use Eq. (30) and write equations for each polarization component. The solution of the linear system of coupled equations can be written in the vector form as

$$\mathbf{p} = -\frac{\mathbf{d}(\mathbf{d}^* \cdot \mathbf{E}^{\text{inc}})}{\hbar(\omega-\omega_0-\delta+i\gamma)}. \tag{37}$$

The frequency shift and radiative decay in Eq. (37) are

$$\frac{\delta}{\gamma_v} = -\frac{1}{g_v}\sum_{i=\rho,\varphi,z} n_i^2\, \text{Re}\, G_{ii}^{(1)}, \tag{38a}$$

$$\frac{\gamma}{\gamma_v} = \sqrt{\varepsilon} + \frac{1}{g_v}\sum_{i=\rho,\varphi,z} n_i^2\, \text{Im}\, G_{ii}^{(1)}, \tag{38b}$$

where n_i are the projections of the unit vector $\hat{\mathbf{n}}$ which defines the dipole direction $\mathbf{d} = \hat{\mathbf{n}}d$. Equations (37) and (38) generalize Eqs. (34) and (35) for an arbitrary scatterer orientation defined by $\hat{\mathbf{n}}$. The polarization in Eq. (37) can be oriented not only along the components of the incident field $\mathbf{E}^{\text{inc}}$ but also in other directions. In general, this leads to the conversion between the linearly polarized modes (2), in other words, the incidence of a linearly polarized guided mode results in two transmitted and two reflected modes. However, when the dipole moment has only ρ and z components, it still interacts only with the x-polarized mode.

E. Transmission, reflection, and bulk scattering

1. Excitation of guided waves

The derived formulas for the self-consistent polarization (33)–(35) in combination with the solution of the dipole emission problem are sufficient to find the required transmission, reflection, and bulk scattering (see Sec. II A). However, simple analytical formulas can be derived in the single mode regime, which is realized when a linearly polarized mode is incident on the scatterer [see Eq. (2)]. The analytical formulas for the transmission, reflection, and bulk scattering will be expressed in terms of two parameters which can be obtained by studying the dipole emission only: the fraction of emission into the guided modes β and the enhancement of the total emission γ/γ_v.

Let us first find the amplitudes of the guided waves excited by the point source (11). Since the Green's function gives the self-consistent polarization, one can calculate the amplitudes of the excited guided waves. We take the incident guided wave as

$$\mathbf{E}^{\text{inc}}(\mathbf{r}) = A_0\boldsymbol{\mathcal{E}}^+(\rho,\varphi)e^{ih_g z} \tag{39}$$

and the excited waves as

$$\mathbf{E}_g^\pm(\mathbf{r}) = A^\pm\boldsymbol{\mathcal{E}}^\pm(\rho,\varphi)e^{\pm ih_g z}, \tag{40}$$

where $h_g > 0$ is the wave number, $\boldsymbol{\mathcal{E}}^\pm(\rho,\varphi)$ are the spatial distributions for the $\pm z$ guided waves, A_0 is the amplitude of the incident wave, and $A^\pm$ are the amplitudes of the excited waves. We choose $\boldsymbol{\mathcal{E}}^- = (\boldsymbol{\mathcal{E}}^+)^*$. To find $A^\pm$ we can write the power generated by the polarization $\mathbf{p}$ using two ways. First, we can represent it as

$$P_g^\pm = P_1|A^\pm|^2, \tag{41}$$

where P_1 is the power for $|A^\pm| = 1$. The power P_1 can be considered as some normalization for the modal profiles $\boldsymbol{\mathcal{E}}^\pm(\rho,\varphi)$ and can be included directly into their definition. Second, we can use Eq. (20) to write

$$P_g^\pm = -i\omega A^\pm(\mathbf{p}^* \cdot \boldsymbol{\mathcal{E}}^\pm), \tag{42}$$

where the value of the modal field $\boldsymbol{\mathcal{E}}^{\pm}$ is evaluated at the scatterer location. Equating (41) and (42) we obtain the amplitudes

$$A^{\pm} = \frac{i\omega}{P_1}\mathbf{p}\cdot\boldsymbol{\mathcal{E}}^{\mp}. \tag{43}$$

The power of the guided waves excited by $\mathbf{p}$ becomes

$$P_g^{\pm} = \frac{\omega^2}{P_1}|\mathbf{p}\cdot\boldsymbol{\mathcal{E}}^{\mp}|^2. \tag{44}$$

The knowledge of the excited amplitudes (43) can also be used to find the emission in a waveguide of finite length. If the emitter is far away from the ends, their presence does not modify the emission into the bulk waves which rather quickly leave the waveguide. The ends form a cavity for the guided modes and the emission into the cavity modes can be calculated by considering multiple reflections of the excited guided modes from the ends [31]. The reflection coefficients for the guided modes can be calculated numerically [33]. In principle, some leaky modes can also travel rather large distances [31] and their role can also be included using their reflectivities as well. If the ends are close to the emitter, one can resort to finding the Green's function for the emitter inside the finite-length cylinder [34].

We can now use the self-consistent polarization to express the amplitudes of the excited waves (43) in terms of the amplitude of the incident wave.

2. Scatterer oriented along a basis direction

For a scatterer oriented along one of $\hat{\boldsymbol{\rho}}$, $\hat{\boldsymbol{\varphi}}$, or $\hat{\mathbf{z}}$ we obtain from Eqs. (33) and (34) the following polarization:

$$p_j = -\frac{\gamma_v A_0 \mathcal{E}_j^+}{g_v(\omega-\omega_0-\delta_j+i\gamma_j)}, \quad j=\rho,\varphi,z. \tag{45}$$

Substituting (45) into (43) gives

$$\frac{A_j^+}{A_0} = -i\frac{\beta_j\gamma_j}{\omega-\omega_0-\delta_j+i\gamma_j}, \quad \frac{A_j^-}{A_0} = \frac{A_j^+}{A_0}\cdot\frac{\mathcal{E}_j^+}{\mathcal{E}_j^-}. \tag{46}$$

In (46) we introduced the decay rate $\beta_j\gamma_j$ for the dipole due to the emission into the guided modes:

$$\beta_j\gamma_j = \frac{2P_g^+}{P_{\text{tot}}}\frac{P_{\text{tot}}}{P_v}\gamma_v = \frac{\omega\gamma_v|\mathcal{E}_j^+|^2}{P_1 g_v}, \tag{47}$$

where we used (18) and (44).

The transmission $T=|1+A^+/A_0|^2$, the reflection $R=|A^-/A_0|^2$, and the power $S=P_b/P_0$ scattered into bulk waves can now be written using $A_j^{\pm}$ given by (46) as

$$T = 1-\beta_j(2-\beta_j)\mathcal{L}_j(\omega), \tag{48a}$$

$$R = \beta_j^2\mathcal{L}_j(\omega), \tag{48b}$$

$$S = 2\beta_j(1-\beta_j)\mathcal{L}_j(\omega), \tag{48c}$$

where

$$\mathcal{L}_j(\omega) = \frac{\gamma_j^2}{(\omega-\omega_0-\delta_j)^2+\gamma_j^2} \tag{49}$$

is the Lorentzian line-shape factor for the given dipole orientation. Its value at the shifted resonance is $\mathcal{L}_j(\omega_0+\delta_j)=1$. Thus, according to Eq. (48), all scattering properties for a specific dipole orientation along a basis vector are defined by the corresponding β_j factor and the radiative decay rate γ_j. The radiative decay γ_j can be written as a product of two factors: the enhancement of power emission γ_j/γ_v, which depends only on the electromagnetic interaction, and the radiative decay rate in vacuum γ_v, which depends on the dipole moment.

The values of T, R, and S [see Eq. (48)] at resonance can be obtained using a simpler way with some prior knowledge at hand. Indeed, the incident mode with amplitude A_0 induces scatterer polarization which in turn excites new guided waves with amplitudes $A_j^{\pm}$ (with $j=\rho$, φ, or z denoting the orientation of the transition dipole moment) propagating in the $\pm z$ directions and bulk radiation. The power balance yields

$$|A_0|^2 = |A_0+A_j^+|^2+|A_j^-|^2+(|A_j^+|^2+|A_j^-|^2)\frac{1-\beta_j}{\beta_j},$$

where the last term relates the bulk radiation to the excited waves. If A_j^+/A_0 is real at resonance [see Eq. (46)] and $|A_j^+|=|A_j^-|$ [see Eq. (43)], the balance equation gives $A_j^+/A_0=-\beta$, from which the resonant values are $T=(1-\beta_j)^2$, $R=\beta_j^2$, and $S=2\beta_j(1-\beta_j)$, in agreement with Eq. (48).

3. Isotropic scatterer

For an isotropic scatterer the polarization $\mathbf{p}$ has three independent terms [see Eq. (36)], describing each component separately. The polarization excites guided modes propagating in the $\pm z$ directions. The transmitted signal is the sum of the initial wave and the wave generated by the scatterer polarization. Each polarization component contributes to the excitation. The amplitude A^+ of the excited $+z$ wave can be written as a sum $A^+=A_\rho^+ + A_\varphi^+ + A_z^+$, where A_j^+ is the amplitude excited by p_j and defined by Eq. (46). Note that each contribution has different parameters: δ_j, γ_j, and β_j. While the line shape which corresponds to any single component is Lorentzian, their superposition can produce a complicated line shape analyzed in Sec. III C.

F. Optomechanical properties

1. Propelling force and linear momentum flux

There are several ways to find the propelling force on the scatterer and we consider here three of them. The first way is to apply the Lorentz formula with both the electric and magnetic parts for the force on a dipole:

$$F_z = p_x\frac{\partial E_z}{\partial x}+p_y\frac{\partial E_z}{\partial y}+p_z\frac{\partial E_z}{\partial z}+\frac{1}{c}(j_xB_y-j_yB_x) \tag{50}$$

where $\mathbf{E}$ and $\mathbf{B}$ are the true fields at the dipole location. Using the complex fields and expressing $B_{x,y}$ in terms of the spatial derivatives of $\mathbf{E}$ from the Maxwell equations we obtain the time-averaged force:

$$F_z = 2\,\text{Re}\left[p_x^*\frac{\partial E_x}{\partial z}+p_y^*\frac{\partial E_y}{\partial z}+p_z^*\frac{\partial E_z}{\partial z}\right]. \tag{51}$$

Similar formulas were also used in Ref. [35]. The electric field in Eq. (51) includes the incident field as well as the field created due to the interaction with the wire. However, the

symmetry of the Green's function in the considered geometry allows some simplification of Eq. (51). In particular, for the dipole orientation along any of the basis directions the force is

$$F_z = 2h_g\left|E_j^{\rm inc}\right|^2 {\rm Im}\,\chi_j, \quad j = \rho,\ \varphi,\ z. \tag{52}$$

Equation (52) also works in multimode regimes.

The second way is to use the difference between the linear electromagnetic momentum flux along the z direction of the incident wave and all scattered waves. In general, the momentum flux of the scattered bulk waves can have some component along the z direction. However, a dipole oriented along any of the basis directions emits bulk waves symmetrically in the $+z$ and $-z$ directions. Therefore, the z component of the momentum flux of bulk waves equals zero. In the single mode regime, this allows finding the propelling force from the following difference:

$$F_z = M_0 - M_0(T - R) = M_0(1 - T + R), \tag{53}$$

where M_0 is the incident momentum flux, which can be calculated in several ways as discussed in Sec. II B; T is the transmission; and R is the reflection coefficient for a given dipole orientation [see Eqs. (48)].

The third way is to simplify Eq. (53) further using the analytical results for R and T in the single mode regime given by Eqs. (48). Substituting Eqs. (48) into (53) gives

$$\frac{F_z}{M_0} = 2\beta_j \mathcal{L}_j(\omega). \tag{54}$$

Thus, the force can be directly calculated using the β factor in the single mode regime. It follows from Eq. (54) that the resonant propulsion is $F_z = 2M_0\beta_j$. The largest possible value $F_z = 2M_0$ is achieved in the ultimate coupling limit $\beta_j = 1$, when the incident mode is fully reflected.

The calculation of the force requires using the pseudomomentum (due to Minkowski), rather than the electromagnetic momentum (due to Abraham). This was previously verified for the forces on arbitrary size circular scatterers created by the incident surface wave of a metal boundary [36], by a guided mode of a metal layer [37] or a dielectric waveguide [38].

2. Torque and angular momentum flux

The torque on the scatterer can be found using the approaches similar to that for the force. The first way is to calculate the φ component of the force and then use it to find the z component of the torque:

$$T_z = x_0 F_\varphi, \quad F_\varphi = 2{\rm Re}\left[p_j^* \frac{\partial E_j^{\rm inc}}{\partial \varphi}\right]. \tag{55}$$

The second way is to use the difference between the angular momentum flux of the incident wave along the z direction and all scattered waves. Note that the scattering of a linearly polarized wave does not create any torque. The scattering of the circularly polarized $n = +1$ wave produces the transmitted and reflected $n = \pm 1$ waves. The z component of the angular momentum of the bulk waves vanishes because of the symmetry of the emission created by the dipole oriented along the basis directions. The torque becomes

$$\begin{aligned} T_z &= J_0(1 - T_{n=+1} + T_{n=-1} - R_{n=+1} + R_{n=-1}) \\ &= J_0(1 - T_{n=+1} + T_{n=-1}), \end{aligned} \tag{56}$$

where J_0 is the incident angular momentum flux discussed in Sec. II B, $T_{n=\pm1}$ and $R_{n=\pm1}$ are the powers (normalized to the incident) of the transmitted and reflected $n = \pm 1$ modes, and $R_{n=+1} = R_{n=-1}$ due to symmetry.

The third way is to simplify Eq. (56) by expressing the transmissions $T_{n=\pm1}$ in terms of β_j. The incidence of the $n = +1$ mode with amplitude A_0 gives rise to two $n = +1$ waves with amplitudes $A^{\pm}_{n=+1}$ and two $n = -1$ waves with amplitudes $A^{\pm}_{n=-1}$. Similar to the balance considered in Sec. II E 2, we express the bulk radiation in terms of the guided amplitudes and use $|A^+_{n=+1}| = |A^-_{n=+1}| = |A^+_{n=-1}| = |A^-_{n=-1}|$:

$$|A_0|^2 = |A_0 + A^+_{n=+1}|^2 + 3|A^+_{n=+1}| + 4|A^+_{n=+1}|^2 \frac{1-\beta_j}{\beta_j}.$$

If $A^+_{n=+1}/A_0$ is real at resonance, the balance equation gives $A^+_{n=+1}/A_0 = -\beta_j/2$. Substituting $T_{n=+1} = (1 - \beta_j/2)^2$ and $T_{n=-1} = \beta_j^2/4$ into Eq. (56) and accounting for the Lorentzian profile we obtain

$$\frac{T_z}{J_0} = \beta_j \mathcal{L}_j(\omega). \tag{57}$$

Similar to the force given by Eq. (54), the angular momentum transferred to the resonant scatterer is directly proportional to β_j. Unlike the force, the resonant torque is only $T_z = J_0\beta_j$ due to the intermode conversion.

III. RESULTS AND ANALYSIS

A. Dipole source: Emitted power, coupling efficiency, and frequency shifts

Let us first analyze the emission properties of a point source as described in Sec. II C. We consider a wire with $\varepsilon_2 = 6$ (typical for semiconductors) in air with $\varepsilon_1 = 1$. The single mode regime is realized for $kR < 1.075$. For the characterization of resonant scattering later it is sufficient to evaluate the emission properties at the resonant, or operating, frequency since $\gamma_v \ll \omega_0$. For the operating point we chose $kR = 0.9$ for which the phase index for the guided mode is $n_{\rm ph} = 1.293$, and the group index is $n_{\rm gr} = 3.000$. The numerical results presented in the text typically contain three to four significant digits to allow a more accurate verification or benchmarking by the interested reader. The fraction of mode energy per unit length localized inside the wire is 0.689. The fraction of guided power inside is 0.576. Thus, the choice of the operating point provides the single mode guiding regime with good mode confinement.

Figure 2(a) shows the coupling efficiency $\beta_j = P_g/P_{\rm tot}$, where $P_g = P_g^+ + P_g^-$ is the power emitted into the guided modes in both $\pm z$ directions and $P_{\rm tot}$ is the total emitted power for a j-polarized ($j = \rho, \varphi, z$) source. Note that the guided power can be viewed either as the power of the linear mode coupled to the corresponding dipole or the total power of the $n = \pm 1$ circular modes. When the source is outside, $x_0 > R$, then all β_j typically decrease due to the evanescent decay of the guided field. However, β_φ has a rather weak

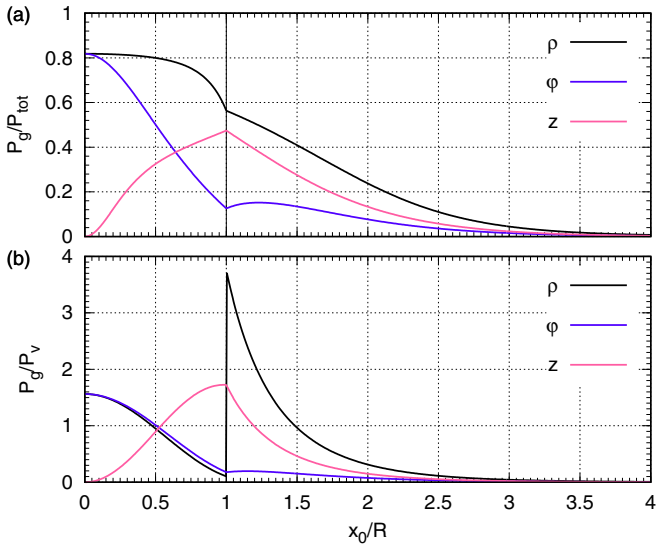

FIG. 2. Power emitted by a dipole oriented along ρ, φ, and z into the guided modes (a) normalized to the total emitted power $P_g/P_{\rm tot} = \beta_j$ and (b) normalized to the power emitted in vacuum P_g/P_v as functions of its location.

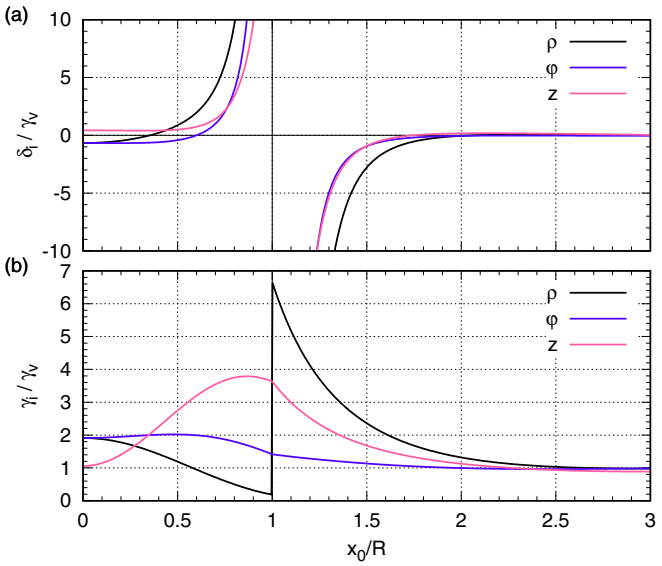

FIG. 3. Normalized (a) frequency shift $\delta_i/\gamma_v = -\mathrm{Re}\, G^{(1)}_{ii}/g_v$ and (b) power enhancement $\gamma_i/\gamma_v = P_{\rm tot}/P_v = \sqrt{\varepsilon} + \mathrm{Im}\, G^{(1)}_{ii}/g_v$ as functions of the dipole location x_0/R for its orientation along ρ, φ, and z directions.

local maximum slightly away from the surface. Depending on dipole orientation, β_j can reach its global maximum either near the boundary, $x_0 = R$ ($\beta_z = 0.474$), or at the center, $x_0 = 0$ ($\beta_{\rho,\varphi} = 0.818$). At $x_0 = 0$, the guided powers for the ρ- and φ-polarized sources are equal while there is no guided emission for the z-polarized source since the axial electric field of the guided modes vanishes.

Figure 2(b) shows the power emission into the guided mode normalized to the power that would be emitted in vacuum P_g/P_v. This quantity is directly proportional to the Purcell factor [see Eq. (24)], except here the enhancement relative to vacuum is used, which is more convenient for analyzing the cases $x_0/R < 1$ and $x_0/R > 1$ simultaneously. To find the conventional $F_{\rm P}$ one can simply divide the plotted quantity P_g/P_v by ε_2 at $x_0 < R$. The ρ-polarized dipole gives the largest enhancement $P_g/P_v = 3.75$ just outside the wire, and the largest suppression $P_g/P_v = 0.104$ just inside the wire. The value of the jump agrees with the dielectric screening factor $(\varepsilon_2/\varepsilon_1)^2 = 36$. In contrast, the enhancement factors P_g/P_v for the φ-polarized and z-polarized dipoles are continuous at the boundary $x_0 = R$. The z-polarized dipole also gives a rather significant enhancement at the boundary $P_g/P_v = 1.72$.

The field emitted by the dipole source near the wire boundary acts on the dipole itself. If the dipole is not a fixed source but rather a resonant scatterer, this field changes its resonant frequency and the emitted power (see Sec. II D 2). The frequency shift [see Fig. 3(a)] at $x_0 = 0$ can be positive or negative depending on polarization. The shift appears divergent when the scatterer approaches the boundary. This is qualitatively similar to an emitter near a plane boundary in the quasistatic limit where the frequency shift $\approx 1/d^3$, where d is the distance to the boundary [39,40]. Near the curved interface the divergence has a different scaling. However, in practice other effects will influence the frequency shifts at very small distances.

Figure 3(b) shows the enhancement of the emitted power $\gamma_i/\gamma_v = P_{\rm tot}/P_v$ as compared to that in vacuum for various dipole orientations. The same results were obtained by calculating the total emitted power (guided and bulk) and the Green's function at the source location. While the enhancement factor is usually $P_{\rm tot}/P_v > 1$, for the ρ-polarized dipole we observe a significant suppression of emission $P_{\rm tot}/P_v < 1$ in the range $0.58 < x_0/R < 1$. Far away from the wire, the enhancement approaches $P_{\rm tot}/P_v = 1$ but shows some very weak oscillations around this value for all polarizations.

The power emitted by the dipole source polarized tangentially, along φ or z, to the wire surface is continuous at $x_0 = R$. For the ρ-polarized source, the power curve jumps as the source crosses the interface. Note that the power emitted into the guided mode also jumps but the β_ρ factor is continuous ($\beta_\rho = 0.564$) [see Fig. 2(a)]. The maximum emission enhancement is very large, $P_{\rm tot}/P_v = 6.66$, and corresponds to the ρ-polarized source located just outside the wire. In contrast, the emission is greatly suppressed, $P_{\rm tot}/P_v = 0.185$, for the ρ-polarized dipole just inside the wire. Similar to that for the guided waves, the value of the jump in the total emission agrees with the dielectric screening factor $(\varepsilon_2/\varepsilon_1)^2 = 36$. For $x_0 > R$ the emitted power decreases with distance from the wire for all dipole orientations.

B. Scatterer oriented along a basis direction

Let us now turn to studying the interaction of a guided mode with a polarizable scatterer which has its dipole moment oriented along one of the three basis directions ρ, φ, or z. To avoid the intermode scattering and to enable the interaction we use the x-polarized mode for the ρ- and z-oriented dipoles and the y-polarized mode for the φ-oriented dipole.

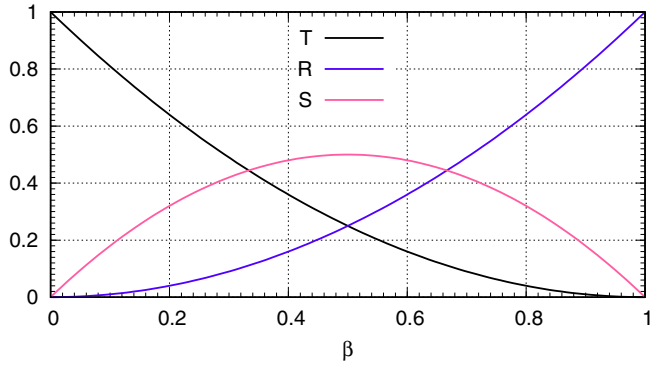

FIG. 4. Guided mode transmission T, reflection R, and scattering S into bulk waves as functions of the β factor for the scatterer at resonance in the single mode regime.

As discussed in Sec. II A, the solution of the emission problem gives the scattered fields (guided and bulk) from the polarizability (34) after the local field is calculated. While this approach is quite general, the use of the β and γ/γ_v factors, also calculated from the emission problem, allows using the simple analytical results presented in Sec. II E 2. Both approaches were implemented and their numerical results matched. This verifies the numerical results as well as the analytical results given by Eqs. (48).

The general dependences of transmission, reflection, and bulk scattering on the β factor in the single mode regime at resonance are described by Eqs. (48) at $\mathcal{L} = 1$ and shown in Fig. 4. The transmission decreases with increasing β, while the reflection increases. The scattering into bulk waves reaches its maximum at $\beta = 0.5$. It is quite remarkable that for large values of $\beta \gtrsim 0.8$ the transmission practically disappears and all incident power goes into reflection and bulk scattering. One can compare this with other situations of transmission through resonant structures. For example, a plane wave incident on a thin resonant film (with plasma or atomic resonance) will be fully reflected at exact resonance. A guided wave coupled to a WGM resonator will be mostly scattered [36,38].

Figure 5 shows the transmission spectrum for various orientations of the scatterer. In all cases the spectrum has a single

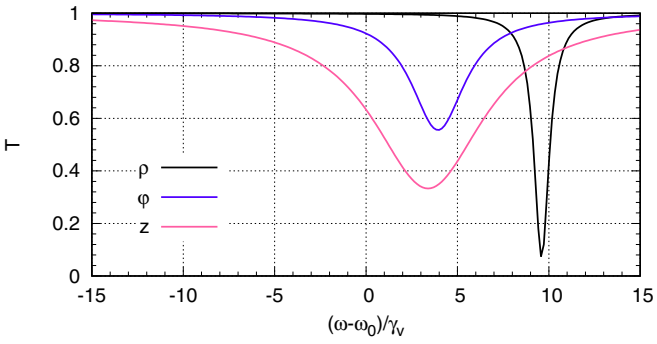

FIG. 5. Transmission spectrum for a linearly polarized guided mode when the dipole scatterer is located at $x_0/R = 0.8$ and oriented along the ρ, φ, or z direction. The incident mode is x polarized for the ρ- and z-oriented dipoles, and y polarized for the φ-oriented ones.

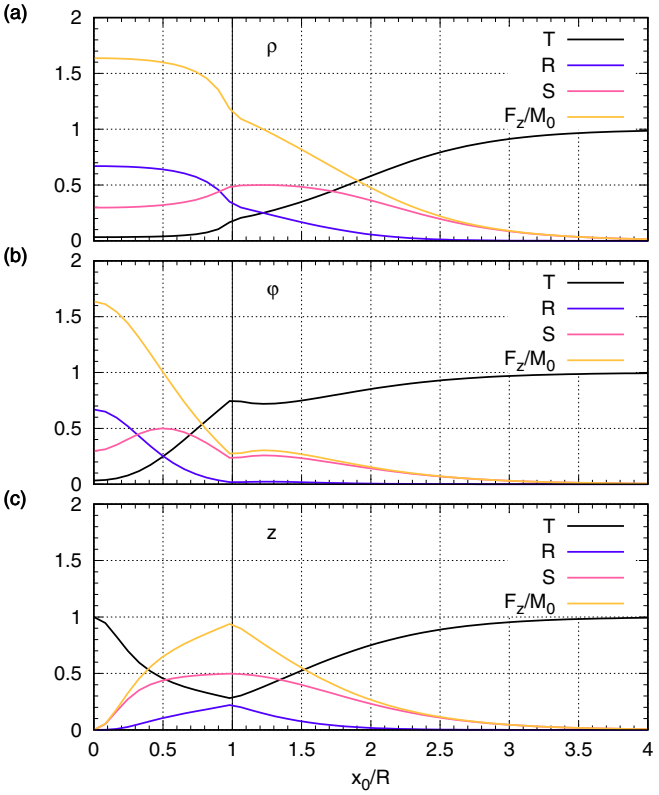

FIG. 6. Transmission T, reflection R, scattering into bulk waves S, and propulsion F_z/M_0 at resonance ($\omega = \omega_0 + \delta_i$) as functions of the scatterer position for three possible orientations: (a) ρ oriented, (b) φ oriented, and (c) z oriented. The incident mode is (a, c) x polarized and (b) y polarized.

Lorentzian dip described by Eq. (48a) with corresponding values of β_j, γ_j, and δ_j, with $j = \rho$, φ, z, which can be obtained from Figs. 2 and 3. The transmission dip for the ρ-oriented scatterer is narrowest and deepest among the three orientations. This corresponds to the lowest total emission [see Fig. 3(b)] and the largest fraction of the emission into the guided mode [see Fig. 2(a)].

Since all scattering characteristics have the Lorentzian frequency dependence, let us look at their values at resonance, where $\mathcal{L} = 1$. Figure 6 shows the dependence of transmission, reflection, bulk scattering, and propulsion as functions of the scatterer location x_0. The propelling force normalized to the momentum flux F_z/M_0 in Fig. 6 was calculated using the three ways described in Sec. II F 1 and the results matched. At $x_0 = 0$ the transmission is very low, $T = 0.0331$, for the ρ- and φ-polarized scatterers, while $T = 1$ for the z-polarized scatterer. When the scatterer is far away from the wire $x_0/R \gg 1$, then $T \to 1$, $R \to 0$, and $S \to 0$ for all orientations. The lowest transmission is obtained for the ρ-polarized scatterer. The low transmission corresponds to large propelling force F_z/M_0. This also follows from the analytical formulas [see Eqs. (48a) and (54)]. The largest force $F_z/M_0 = 1.63$ is obtained for the ρ- and φ-polarized scatterers at the center $x_0 = 0$. For the z-polarized scatterer the largest force $F_z/M_0 = 0.92$ is at $x_0 = R$. The propulsion decreases substantially at large distances $x_0/R \gtrsim 3$ from the wire.

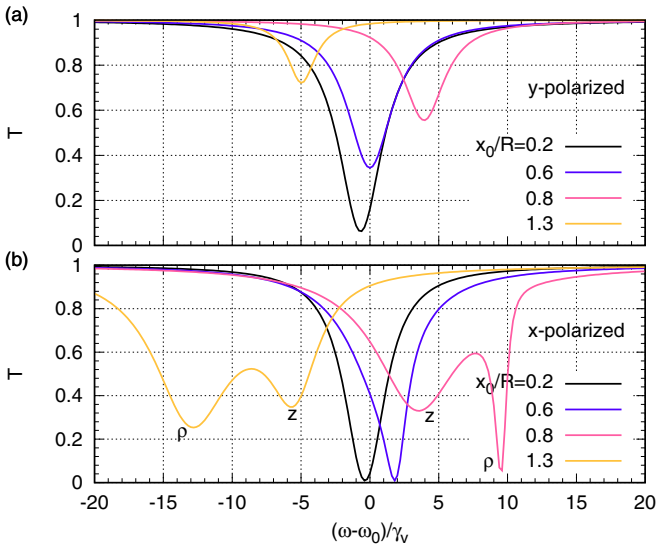

FIG. 7. Transmission spectrum for the x- and y-polarized incident guided modes in the case of an isotropic scatterer at various locations x_0/R. The labels ρ and z near the dips in frame (b) denote the polarization components responsible for their formation.

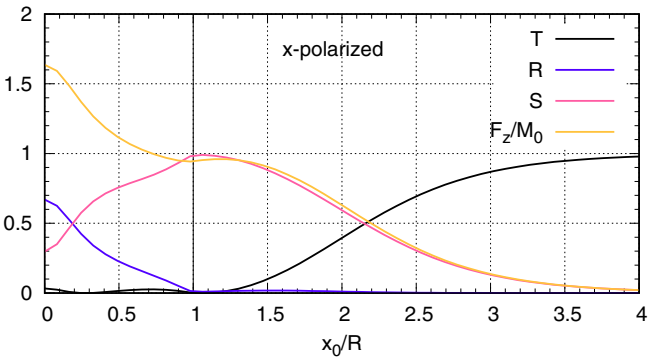

FIG. 8. Transmission T, reflection R, scattering into bulk waves S, and propulsion F_z/M_0 for the x-polarized mode incident on an isotropic scatterer at resonance $\omega = \omega_0$. The shift of the resonant frequency is neglected, $\delta_\rho = \delta_z = 0$.

C. Isotropic scatterer

1. Scattering with frequency shifts

Let us now study how the transmission changes if the scatterer is isotropic, namely, it can be represented as three dipoles oriented along $\hat{\boldsymbol{\rho}}$, $\hat{\boldsymbol{\varphi}}$, and $\hat{\boldsymbol{z}}$. If the incident mode is y polarized [see Fig. 7(a)], the transmission spectrum has one Lorentzian dip because only the φ component of the scatterer polarization is excited. The most pronounced dip is observed for the scatterer at the center. The minimal value of transmission can be evaluated from $T = (1 - \beta_\varphi)^2$ [see Eq. (48a)]. Taking β_φ from Fig. 3, we obtain $\beta_\varphi = 0.818$, $T = 0.0331$ for $x_0 = 0$ and $\beta_\varphi = 0.751$, $T = 0.062$ for $x_0/R = 0.2$. The dip is shifted slightly to the red (to lower frequencies) for $x_0/R < 0.6$, in agreement with the shifts in Fig. 3(a). As the scatterer moves beyond $x_0/R = 0.6$ the dip becomes more shallow and shifts to the blue (to higher frequencies). When the scatterer is moved outside of the wire, the rather shallow transmission deep switches to the lower frequency side, again in full agreement with Fig. 3(a). It is essential that the transmission is always characterized by the Lorentzian line shape.

Figure 7(b) shows the transmission spectrum for the x-polarized mode. In contrast to the y-polarized mode in Fig. 7(a), the x-polarized mode excites the ρ- and z-polarization components, and the transmission, in general, shows two dips with different depths and widths. When the scatterer is near the center, $x_0/R = 0.2$, the transmission dip reaches almost zero and is slightly shifted to the red. For $x_0 \to 0$, the field at the scatterer location has $E_\rho \neq 0$, $E_z = 0$ and the transmission is equal to that in the y-polarized case, $T = 0.0331$. As the scatterer is moved further from the center, the transmission dip shows some noticeable deviations from the Lorentzian line shape due to the growth of the contributions from the z-polarized dipole. When the displacement becomes significant, $x_0/R = 0.8$, the transmission spectrum develops two separated dips. This unusual behavior is due to the presence of two response functions χ_ρ and χ_z, characterized by $\delta_{\rho,z}$ and $\gamma_{\rho,z}$ (see Fig. 3). As x_0 approaches R, γ_ρ decreases (the corresponding dip becomes narrower), while γ_z increases (the corresponding dip becomes wider). Furthermore, since $|\delta_\rho| > |\delta_z|$ the frequency shifts differ. This means that the transmission spectrum should develop two dips and the dip with the larger blueshift should be narrower. This is indeed observed in Fig. 7(b). As the scatterer moves just outside the wire, γ_ρ jumps to a higher value and the corresponding dip broadens. A further increase of x_0, $x_0/R \to \infty$, leads to a merger and disappearance of the two dips.

2. Scattering without frequency shifts

In the previous section it was shown that for a typical strongly guided mode, which has several field components with comparable values, the transmission spectrum becomes quite complicated, showing multiple different dips for a resonant isotropic scatterer. These results are based on the two-level model (see Sec. II D). Real emitters have more than two levels and, therefore, it may not be a realistic model to describe all properties [41]. The inadmissibility of the two-level model treating frequency shifts near interfaces is highlighted in Ref. [42], where significantly smaller shifts are estimated. Indeed, experimental measurements can give frequency shifts significantly smaller or even of different signs [43]. Since it is expected that the two-level model may significantly overestimate the shifts near interfaces, let us assume that the shifts are negligible and study the effects of the broadening alone, for which the two-level model is adequate.

The scattering of the y-polarized mode reduces to the case in which the dipole is oriented along the φ direction [see Fig. 6(b)]. The transmission spectrum is described by Fig. 7(a) but without the frequency shifts.

For the x-polarized mode (see Fig. 8), two polarization components are excited coherently and, therefore, the characteristics will differ from that for a dipole oriented along one of these directions. An interesting feature of Fig. 8 is that the transmission is very low for any location of the scatterer inside the wire, $x_0/R < 1$, and even outside for $1 < x_0/R \lesssim 1.3$. Such a large range of x_0/R with small transmission does not take place for a scatterer with a specific orientation. Using the

results of Secs. II D 3 and II E 2, the resonant transmission can be written as

$$T = (1 - \beta_r - \beta_z)^2. \tag{58}$$

Since $0 < \beta_{\rho,z} < 1$, then $T < 1$. Interestingly, we can obtain $T = 0$ when $\beta_r + \beta_z = 1$. This condition is met at $x_0/R = 0.274$ and 1.055. The addition of β_r and β_z explains the small transmission in a wide range of x_0/R since while each of $\beta_{\rho,z}$ changes significantly their sum has much smaller variation $0.8 < \beta_r + \beta_z < 1.2$ for $0 < x_0/R < 1.3$. The reflection drops very rapidly with increasing displacement of the scatterer from the center and is practically zero when it is outside the wire. The resonant reflection can be written as

$$R = (\beta_r - \beta_z)^2. \tag{59}$$

While β_r and β_z are added for transmission (58), for reflection (59) they are subtracted and we also have $R < 1$. The subtraction comes from Eq. (46) and the $\pi/2$ phase difference between the $\mathcal{E}_\rho^+$ and $\mathcal{E}_z^+$ components. The propelling force for an isotropic scatterer reaches maximum at the center. In finding the force using the momentum balance for an isotropic scatterer one needs to account for the z component of the bulk radiation which becomes nonzero, unlike in the case of a scatterer oriented along one of the basis directions.

The transmission spectra for the x-polarized mode shown in Fig. 7(b) will also be drastically changed if the frequency shift is absent, which is equivalent to setting $\delta_i = 0$ in Eq. (46). Figure 9(a) compares the transmission spectrum for the y- and x-polarized modes for a displaced scatterer. While for the y-polarized mode the transmission dip is Lorentzian, for the x-polarized mode it clearly has a non-Lorentzian line shape.

To understand how the transmission line shape is formed, Figs. 9(b) and 9(c) show the contributions into the transmitted wave from different components of the polarization. For the y-polarized mode [see Fig. 9(b)], the only nonzero polarization component p_φ excites the $+z$ propagating wave with amplitude A_φ^+. This gives the Lorentzian line shape for the transmitted wave in Fig. 9(a). For the x-polarized mode [see Fig. 9(c)], the two polarization components p_ρ and p_z excite $+z$ waves with amplitudes A_ρ^+ and A_z^+, respectively. The spectra of these amplitudes have significantly different magnitudes and widths. The superposition of these two components gives a very narrow transmission dip with very long tails in Fig. 9(a). This transmission line shape cannot be fitted with one or two Lorentzian shapes (49). Instead, the fitting requires taking a coherent superposition of the complex amplitudes.

It is also important to emphasize that the non-Lorentzian spectra are obtained here due to the presence of several transitions. For the x-polarized mode incident on an isotropic scatterer, two polarizations components p_ρ and p_z are excited, resulting in a non-Lorentzian spectrum as discussed above. However, one can also excite two polarization components if the scatterer has only one transition with its dipole moment in the ρ-z plane (see Sec. II D 4). In the latter case, as seen from Eq. (37), the spectra will be Lorentzian but will depend on the dipole orientation.

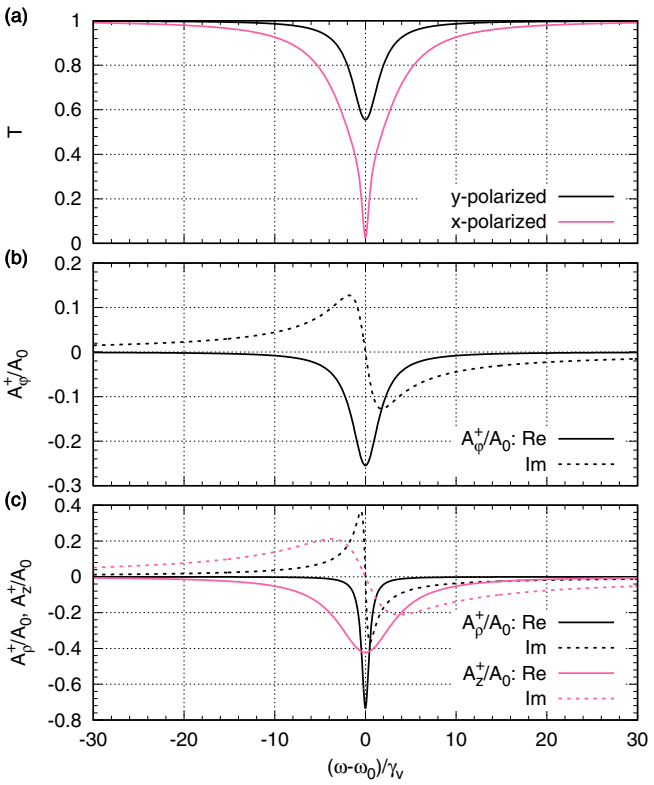

FIG. 9. (a) Transmission spectrum for the linearly y- and x-polarized modes for a displaced $x_0/R = 0.8$ isotropic scatterer at $\delta_i = 0$. (b) Amplitude A_φ^+ of the scattered guided mode in the $+z$ direction excited by the φ component of the scatterer polarization induced by the incident y-polarized mode. (c) Amplitudes $A_{\rho,z}^+$ of the scattered guided modes in the $+z$ direction excited by the ρ and z components of the scatterer polarization induced by the incident x-polarized mode.

D. Torque on the scatterer

Since the incidence of linearly polarized modes considered in the previous sections does not produce any torque on the scatterer, here we consider the incidence of the circularly polarized $n = +1$ mode on a scatterer orientated along one of the basis directions. To find the torque no new calculations are required because, according to Eq. (57), one can use directly the corresponding β factors. The dependence of T_z/J_0 on the scatterer location at resonance for different orientations coincides with the β factors shown in Fig. 2(a). It was verified numerically that all three methods of calculating the torque described in Sec. II F 2 give the same result: using the force in Eqs. (55), angular momentum fluxes in Eq. (56), and β factors in Eq. (57). The torque is maximum when the scatterer approaches the wire axis and is oriented perpendicularly to the propagation direction z. The torque on the z-oriented dipole is zero at $x_0/R \to 0$ but increases as it moves from the axis. When the dipole is outside of the wire, the torque decreases for all three orientations.

IV. CONCLUSION

To conclude, the scattering of a dielectric wire mode on a resonant scatterer was investigated. The resonant scatterer

was modeled as a two-level atom that interacts with the field through a dipolelike transition. The single mode regime was investigated in detail. The use of a dielectric wire made of a semiconductor material allows one to obtain well-confined modes even when the diameter is only a fraction of the operating wavelength. This in turn enables a very efficient interaction of the guided mode with a resonant scatterer located either inside the wire or in its proximity outside.

For a scatterer oriented along a basis direction, all scattering characteristics (transmission, reflection, and bulk scattering) have Lorentzian line shapes, which can be parametrized by their values at resonance, frequency shifts, and widths [see Eqs. (48)]. The parameters of the spectra can be obtained directly from the properties of dipole emission. Without polarization dephasing, the resonance values of transmission, reflection, and bulk scattering depend only on the relative power emitted into the guided mode and the widths depend on the total emission rate. The dependence of power emission on the location and polarization of the dipole was also analyzed.

For an isotropic scatterer, which can be modeled as a coherent superposition of three orthogonal transitions, the scattering characteristics become more complicated if the β factors for the basis orientations are comparable. First, if the frequency shifts for each orientation are significantly different, one can observe multipeak characteristics. Near the waveguide interface the frequency shifts diverge. In practice, the correct calculation of the frequency shifts requires going beyond the two-level model. Second, if the frequency shifts are negligible, the characteristics develop strongly non-Lorentzian line shapes due to the coherent superposition of scattered guided waves produced by the different polarization components. Extracting the interaction parameters from such complicated spectra requires the use of the complex amplitudes of the scattered waves described by Eq. (46), which may be quite difficult in practice. An isotropic scatterer also allows us to obtain a much lower transmission as compared to a single-transition scatterer due to the effective addition of the corresponding β factors. The presence of several transitions, in addition to varying the scatterer location or modal fields, can be used to control the scattering characteristics.

Similar to the scattering characteristics, the propelling force and axial torque on the scatterer have Lorentzian line shapes for any basis orientations of the scatterer. Simple formulas for the resonant force and torque were derived [see Eqs. (54) and (57)]. According to these formulas, the resonant force and torque can be directly obtained from the β factors. It was also shown that finding the force and torque requires the use of the Minkowski form for the electromagnetic linear and angular momentum.

ACKNOWLEDGMENT

This work was supported by the Ministry of Science and Higher Education of the Russian Federation (075-15-2020-927).

[1] S. Faez, P. Türschmann, H. R. Haakh, S. Götzinger, and V. Sandoghdar, Coherent Interaction of Light and Single Molecules in a Dielectric Nanoguide, Phys. Rev. Lett. **113**, 213601 (2014).

[2] P. Türschmann, N. Rotenberg, J. Renger, I. Harder, O. Lohse, T. Utikal, S. Götzinger, and V. Sandoghdar, Chip-based all-optical control of single molecules coherently coupled to a nanoguide, Nano Lett. **17**, 4941 (2017).

[3] A. Sipahigil, R. E. Evans, D. D. Sukachev, M. J. Burek, J. Borregaard, M. K. Bhaskar, C. T. Nguyen, J. L. Pacheco, H. A. Atikian, C. Meuwly, R. M. Camacho, F. Jelezko, E. Bielejec, H. Park, M. Lončar, and M. D. Lukin, An integrated diamond nanophotonics platform for quantum-optical networks, Science **354**, 847 (2016).

[4] M. K. Bhaskar, D. D. Sukachev, A. Sipahigil, R. E. Evans, M. J. Burek, C. T. Nguyen, L. J. Rogers, P. Siyushev, M. H. Metsch, H. Park, F. Jelezko, M. Lončar, and M. D. Lukin, Quantum Nonlinear Optics with a Germanium-Vacancy Color Center in a Nanoscale Diamond Waveguide, Phys. Rev. Lett. **118**, 223603 (2017).

[5] E. Vetsch, D. Reitz, G. Sagué, R. Schmidt, S. T. Dawkins, and A. Rauschenbeutel, Optical Interface Created by Laser-Cooled Atoms Trapped in the Evanescent Field Surrounding an Optical Nanofiber, Phys. Rev. Lett. **104**, 203603 (2010).

[6] J. Claudon, J. Bleuse, N. S. Malik, M. Bazin, P. Jaffrennou, P. Lalanne N. Gregersen, C. Sauvan, and J. M. Gérard, A highly efficient single-photon source based on a quantum dot in a photonic nanowire, Nat. Photonics **4**, 174 (2010).

[7] M. Arcari, I. Söllner, A. Javadi, S. Lindskov Hansen, S. Mahmoodian, J. Liu, H. Thyrrestrup, E. H. Lee, J. D. Song, S. Stobbe, and P. Lodahl, Near-Unity Coupling Efficiency of a Quantum Emitter to a Photonic Crystal Waveguide, Phys. Rev. Lett. **113**, 093603 (2014).

[8] P. Domokos, P. Horak, and H. Ritsch, Quantum description of light-pulse scattering on a single atom in waveguides, Phys. Rev. A **65**, 033832 (2002).

[9] P. Türschmann, H. Le Jeannic, S. F. Simonsen, H. R. Haakh, S. Götzinger, V. Sandoghdar, P. Lodahl, and N. Rotenberg, Coherent nonlinear optics of quantum emitters in nanophotonic waveguides, Nanophotonics **8**, 1641 (2019).

[10] D. E. Chang, A. S. Sørensen, E. A. Demler, and M. D. Lukin, A single-photon transistor using nanoscale surface plasmons, Nat. Phys. **3**, 807 (2007).

[11] A. S. Shalin, P. Ginzburg, P. A. Belov, Y. S. Kivshar, and A. V. Zayats, Nano-opto-mechanical effects in plasmonic waveguides, Laser Photonics Rev. **8**, 131 (2014).

[12] A. V. Poshakinskiy and A. N. Poddubny, Optomechanical Kerker Effect, Phys. Rev. X **9**, 011008 (2019).

[13] S. Boissier, R.C. Schofield, L. Jin, A. Ovvyan, S. Nur, F. H. L. Koppens, C. Toninelli, W. H. P. Pernice, K. D. Major, E. A. Hinds, and A. S. Clark, Coherent characterisation of a single molecule in a photonic black box, Nat. Commun. **12**, 706 (2021).

[14] P. Solano, J. A. Grover, Y. Xu, P. Barberis-Blostein, J. N. Munday, L. A. Orozco, W. D. Phillips, and S. L. Rolston, Alignment-dependent decay rate of an atomic dipole near an optical nanofiber, Phys. Rev. A **99**, 013822 (2019).

[15] M. J. Renn, D. Montgomery, O. Vdovin, D. Z. Anderson, C. E. Wieman, and E. A. Cornell, Laser-Guided Atoms in Hollow-Core Optical Fibers, Phys. Rev. Lett. **75**, 3253 (1995).

[16] S. Kawata and T. Tani, Optically driven Mie particles in an evanescent field along a channeled waveguide, Opt. Lett. **21**, 1768 (1996).

[17] S. Gaugiran, S. Gétin, J. M. Fedeli, G. Colas, A. Fuchs, F. Chatelain, and J. Dérouard, Optical manipulation of microparticles and cells on silicon nitride waveguides, Opt. Express **13**, 6956 (2005).

[18] B. S. Schmidt, A. H. J. Yang, D. Erickson, and M. Lipson, Optofluidic trapping and transport on solid core waveguides within a microfluidic device, Opt. Express **15**, 14322 (2007).

[19] Y. Li, O. V. Svitelskiy, A. V. Maslov, D. Carnegie, E. Rafailov, and V. N. Astratov, Giant resonant light forces in microspherical photonics, Light Sci. Appl. **2**, e64 (2013).

[20] Y. Li, A. V. Maslov, N. I. Limberopoulos, A. M. Urbas, and V. N. Astratov, Spectrally resolved resonant propulsion of dielectric microspheres, Laser Photonics Rev. **9**, 263 (2015).

[21] F. L. Kien and T. Busch, Torque of guided light on an atom near an optical nanofiber, Opt. Express **27**, 15046 (2019).

[22] M. F. Picardi, K. Y. Bliokh, F. J. Rodríguez-Fortuño, F. Alpeggiani, and F. Nori, Angular momenta, helicity, and other properties of dielectric-fiber and metallic-wire modes, Optica **5**, 1016 (2018).

[23] M. Liu, D. A. Powell, I. V. Shadrivov, M. Lapine, and Y. S. Kivshar, Self-oscillations in nonlinear torsional metamaterials, New J. Phys. **15**, 073036 (2013).

[24] T. A. Morgado, S. I. Maslovski, and M. G. Silveirinha, Ultrahigh Casimir interaction torque in nanowire systems, Opt. Express **21**, 14943 (2013).

[25] M. A. Gorlach, A. N. Poddubny, and P. A. Belov, Self-induced torque in discrete uniaxial metamaterials, Phys. Rev. B **90**, 035106 (2014).

[26] A. S. Shalin, S. V. Sukhov, A. A. Bogdanov, P. A. Belov, and P. Ginzburg, Optical pulling forces in hyperbolic metamaterials, Phys. Rev. A **91**, 063830 (2015).

[27] J. P. Gordon, Radiation forces and momenta in dielectric media, Phys. Rev. A **8**, 14 (1973).

[28] F. N. H. Robinson, Electromagnetic stress and momentum in matter, Phys. Rep. **16**, 313 (1975).

[29] H. A. Haus and H. Kogelnik, Electromagnetic momentum and momentum flow in dielectric waveguides, J. Opt. Soc. Am. **66**, 320 (1976).

[30] M. Partanen and J. Tulkki, Light-driven mass density wave dynamics in optical fibers, Opt. Express **26**, 22046 (2018).

[31] A. V. Maslov, M. I. Bakunov, and C. Z. Ning, Distribution of optical emission between guided modes and free space in a semiconductor nanowire, J. Appl. Phys. **99**, 024314 (2006).

[32] A. V. Maslov, Binding of resonant dielectric particles to metal surfaces using plasmons, Ann. Phys. (Berlin) **532**, 2000129 (2020).

[33] A. V. Maslov and C. Z. Ning, Reflection of guided modes in a semiconductor nanowire laser, Appl. Phys. Lett. **83**, 1237 (2003).

[34] V. Bordo, Purcell factor for a cylindrical nanocavity: Ab initio analytical approach, J. Opt. Soc. Am. B **29**, 1799 (2012).

[35] P. C. Chaumet and M. Nieto-Vesperinas, Time-averaged total force on a dipolar sphere in an electromagnetic field, Opt. Lett. **25**, 1065 (2000).

[36] A. V. Maslov, V. N. Astratov, and M. I. Bakunov, Resonant propulsion of a microparticle by a surface wave, Phys. Rev. A **87**, 053848 (2013).

[37] A. V. Maslov, Resonant Pulling of a Microparticle Using a Backward Surface Wave, Phys. Rev. Lett. **112**, 113903 (2014).

[38] A. V. Maslov, Optomechanical properties of a particle-waveguide system, Phys. Rev. A **90**, 033825 (2014).

[39] J. M. Wylie and J. E. Sipe, Quantum electrodynamics near an interface, Phys. Rev. A **30**, 1185 (1984).

[40] V. V. Klimov, M. Ducloy, and V. S. Letokhov, Radiative frequency shift and linewidth of an atom dipole in the vicinity of a dielectric microsphere, J. Mod. Opt. **43**, 2251 (1996).

[41] W. L. Barnes, Fluorescence near interfaces: The role of photonic mode density, J. Mod. Opt. **45**, 661 (1998).

[42] G. Barton, Frequency shifts near an interface: Inadequacy of two-level atomic models, J. Phys. B **7**, 2134 (1974).

[43] F. Balzer, V. G. Bordo, and H.-G. Rubahn, Frequency shifts and lifetime changes of sodium atoms near rough metal surfaces, Opt. Lett. **22**, 1262 (1997).